Gas Processing Journal

Vol. 8, No. 2, 2020, pp. 35-50
http://gpj.ui.ac.ir

DOI: http://dx.doi.org/10.22108/gpj.2020.120195.1080

Investigation of methane adsorption on molecular sieve zeolite (from natural materials)

Hossein Esfandian*[1], Vahid Garshasbi[2]

[1] Faculty of Engineering Technologies, Amol University of Special Modern Technologies, Amol, Iran
[2] Faculty of Chemistry, Iran University of Science and Technology, Tehran, Iran

Received: 2020-02-29 Revised: 2020-07-09 Accepted: 2020-07-11

Abstract: In this study, Kaolin, Bentonite, and Feldspar were used as a low-cost source of Si and Al to synthesize the molecular sieve 13X. The synthesized Zeolites were characterized by XRD, FTIR, SEM, TGA, and BET analysis and used as a suitable adsorbent for CH4 adsorption. The surface areas were 591, 505, 472, and 588 m2/g for natural kaolin (13X-K), bentonite (13X-B), feldspar (13X-F) and commercial molecular sieve 13X (13X–C), respectively. The 13X-K had the highest thermal stability than 13X-B and 13X-F. The adsorption capacities (pressure >20bar) of 13X (kaolin), 13X (bentonite), and 13X(feldspar) were 3.6, 2.4, and 1.95 mmol/g, respectively. The adsorption data were fitted to some isotherms including Langmuir, Freundlich, Sips, BET, and Toth. It was found that the Sips model showed better fitting in comparison to other models. The thermodynamic of adsorption was also investigated; the positive value of ΔS_ads^0 revealed the increased randomness at the solid-solution interface during the gas adsorption. The thermodynamic study also indicated that the adsorption process was exothermic and spontaneous. The adsorption capacities of synthesized 13X samples were compared to other adsorbents; it was found that 13X–K showed considerable performance and can be introduced as a suitable adsorbent for applications on a large scale.

keywords: Methane; 13X; Adsorption; Isotherm; Thermodynamic.

1. Introduction

Among the different technologies used for the separation and capturing of carbon dioxide and methane gases, the adsorption process is increasingly competitive because of low maintenance, cost-effectiveness, low energy requirement, and ease of use. (Pires et al., 2008). Various types of adsorbents such as alumina (Delgado et al., 2006), carbons (Llano-Restrepo, 2010; Lee and Park, 2015), metal-organic frameworks (MOFs) (Alaie et al., 2015; Hesas et al., 2015), and molecular sieves (Chen et al., 2014) are used for the removal of CH_4 and CO_2 from the gas stream.

Among the adsorbents, molecular sieves and zeolites are widely considered due to high stability, performance, and low cost. (Lee et al., 2002; Alshameri et al., 2014; Esfandian, 2015; Esfandian et al., 2016b; Opanasenko et al., 2016; Esfandian et al., 2017; Garshasbi et al., 2017). In molecular sieves, the sodium form of the type X crystal (called 13X) is widely used for gas adsorption processes due to high crystallinity and porosity (Bandarchian and Anbia, 2015; Abate et al., 2016; Bacsik et al., 2016). Generally, zeolites are synthesized from sodium aluminosilicate gel formed from various silica and alumina sources using the hydrothermal method. However, the preparation of synthetic zeolites from the chemical source of silica and alumina is expensive. In order to reduce costs, numerous researches are seeking cheap raw materials such as paper sludge (Wajima et al., 2006; Purnomo et al., 2012; Ansari et al., 2014), slag of lithium (Chen et al., 2012b), high silicon fly ash (Kazemian et al., 2010), shale ash of oil (Machado and Miotto, 2005), coal fly ash (Tanaka and Fujii, 2009) bentonite (Ma et al., 2014a), kaolinite and waste porcelain (Ma et al., 2014a; Wang et al., 2014). Among the mentioned sources, Feldspars, kaolin, and bentonite are used for the synthesis of 13X due to the lower costs, availability, and some special properties (Blatt et al., 2006; Holmes et al., 2011; Chen et al., 2014; Ma et al., 2014a).

* Corresponding Author.
Authors' Email Address: [1] H. Esfandian (hossein.esfandian@gmail.com), [2] V. Garshasbi (garshasbi@iust.ac.ir),
ISSN (Online): 2345-4172, ISSN (Print): 2322-3251

Several studies reported the synthesis of the 13X from natural sources but the reported adsorption capacities were not considerable. Ma et al. reported the synthesis of 13X from low-grade natural kaolin via alkali fusion followed by a hydrothermal process. The effect of different parameters, such as NaOH addition amount and crystallization time, on the crystallinity of products, was systematically investigated (Ma et al., 2014b). In other papers, 13X was synthesized using bentonite as the raw material by alkaline fusion followed by a hydrothermal process and used for CO_2 capturing. The synthesized 13X performance was also compared to the commercial ones; the synthesized sample showed lower adsorption capacity (Chen et al., 2014; Ma et al., 2014a).

In this paper, molecular sieve 13X was synthesized by the hydrothermal method using some natural materials such as kaolin, bentonite, and feldspar to adsorb CH4 over a temperature range. The effects of various operational parameters including molar ratio, temperature, time of reaction on the crystallization, and the purity of the synthesized product have been studied. Furthermore, the properties of the synthesized samples, such as crystal morphology, framework structure, and pore structure were characterized by SEM, FT-IR, XRD, TGA, and BET methods. The experimental data of CH_4 adsorption were also fitted to some isotherm models including Langmuir, Sips, Toth, BET, and Freundlich isotherm models to determine the physicochemical properties, such as the adsorption capacity. Finally, the adsorption capacities of synthesized samples were compared with the other adsorbents.

2. Materials and methods

2.1. Preparation of adsorbent

Due to the high content of SiO_2, the natural materials (kaolin, bentonite, and feldspar) should be treated by the acidizing method to achieve 13X. Table 1 shows the main properties of raw and modified natural materials. The obtained mixture gel was stirred for 120 h with magnetic stirring at room temperature and then a homogenous solution was transferred into a Teflon-Lined autoclave for crystallization at the temperature of 65 ± 5 °C for 72h. The products were filtered, washed several times with distilled water (until pH of supernatant reached 9), and dried in the oven at 80 °C for 12 h.

Table 1. Natural materials properties

Main composition	Content (wt%)					
	Kaolin	Modified kaolin	Bentonite	Modified bentonite	Feldspar	Modified feldspar
SiO_2	74.98	56.40	68.85	55.35	69.37	56.28
Al_2O_3	17.42	31.68	18.80	30.95	9.83	31.02

2.2. Characterization Methods

The X-ray Fluorescence (XRF) was used for the characterization of the chemical composition of kaolin, bentonite, and feldspar by a Wavelength X-ray dispersive Fluorescence Spectrometer (Model Bruker S4). The X-ray diffraction (XRD) analysis was employed to characterize the structure of the samples with a GBC MMA diffractometer (CuKa) (model Philips PW1140/90).

The bonds of the natural kaolin, bentonite, feldspar, and molecular sieve 13X were obtained using the FT-IR spectrometer (Perkin-Elmer). The scanning electron microscopy (SEM) was used to investigate the morphological features of the natural and synthesized zeolites. TGA (Thermogravimetric Analysis) was used to check the thermal behavior of the products. Brunauer-Emmett-Teller (BET) surface area analysis was used to calculate pore size distribution, pore diameter, and specific surface area at liquid nitrogen temperature (77 K).

2.3. Experimental Design by Taguchi

Experimental design by the Taguchi method is a well-known tool for the optimization of the multifactor process (Garshasbi et al., 2017). The experimental design of these experiments and the response were achieved using the option of Automatic Design in Qualitek-4 software featuring an L9 orthogonal array with 9 trails. The experimental conditions for the synthesis of the different types of 13X are presented in Table 2.

Table 2. DOE for synthesized molecular sieve according to Taguchi L9 array

Adsorbent	Sample No.	Experiment condition			
		Al2O3/ SiO2	Na2O/Al2O3	Time (h)	Temperature (^{0} C)
13X - K	K1	0.2	3.7	40	65
	K2	0.3	4.7	80	75
	K3	0.4	5.7	120	85
	K4	0.2	3.7	40	65
	K5	0.3	4.7	80	75
	K6	0.4	5.7	120	85
	K7	0.2	3.7	40	65
	K8	0.3	4.7	80	75
	K9	0.4	5.7	120	85
13X - B	B1	0.2	3.7	40	65
	B1	0.3	4.7	80	75
	B1	0.4	5.7	120	85
	B1	0.2	3.7	40	65
	B1	0.3	4.7	80	75
	B1	0.4	5.7	120	85
	B1	0.2	3.7	40	65
	B1	0.3	4.7	80	75
	B1	0.4	5.7	120	85
13X - F	F1	0.2	3.7	40	65
	F1	0.3	4.7	80	75
	F1	0.4	5.7	120	85
	F1	0.2	3.7	40	65
	F1	0.3	4.7	80	75
	F1	0.4	5.7	120	85
	F1	0.2	3.7	40	65
	F1	0.3	4.7	80	75
	F1	0.4	5.7	120	85

2.4. Isotherm Models

The adsorption isotherms are the fundamental requirements for optimizing adsorption systems (Colina et al., 2001). The experimental data of CH_4 adsorption onto 13X samples were fitted to some standard isotherm models to examine the model's constants adsorption isotherms.

2.5. Langmuir isotherm

The Langmuir isotherm model is based on the four assumptions: (a) a fixed number of sites for the adsorption, (b) identical sites, (c) monolayer adsorption, and (d) no interaction between adsorbate molecules. The Langmuir isotherm equation is defined as the following equation (Ladshaw et al., 2015):

$$\frac{q_i}{q_{mi}} = \frac{bP}{bP+1} \quad (1)$$

Where b and q_{mi} are the equilibrium constant and monolayer maximum adsorption capacity, respectively.

2.5.1. Sips Equation

Sips isotherm model is based on localized adsorption without considering adsorbate-adsorbate interactions. The Sips isotherm was formed by a combination of the Langmuir and Freundlich expressions. At low concentrations, Sips convert to Freundlich isotherm whereas, at high concentrations, it behaves as the Langmuir isotherm. The adsorption isotherm model is presented as the following equation (Tzabar and ter Brake, 2016):

$$\frac{q_i}{q_{mi}} = \frac{(bP)^{1/n}}{1+(bP)^{1/n}} \quad (2)$$

$$b = b_0 exp\left[\frac{Q}{RT_0}\left(\frac{T_0}{T}-1\right)\right] \quad (3)$$

$$\frac{1}{n} = \frac{1}{n_0} + \alpha\left(1+\frac{T_0}{T}\right) \quad (4)$$

Where P is the pressure, q_{mi} (mol/Kg) is the maximum adsorption capacity, b is the sorption affinity, and n as a dimensionless parameter is related to the heterogeneity of the adsorbate-adsorbent process. Q and b_0 are the isosteric heat of sorption at half loading and the constant of adsorption at the temperature T_0 respectively. The dependency of heterogeneity parameter (n) to the temperature is described by n_0 and α parameters.

2.5.2. Toth Isotherm

The Toth isotherm is a semi-empirical expression obtained by extending the Langmuir equation and considering the heterogeneity of adsorbent surfaces (Toth, 2002). The three parameters Toth isotherm is based on a quasi-Gaussian energy distribution which can be introduced as the most useful isotherm in describing the heterogeneous

adsorption systems of gases at a wide range of pressure. Toth isotherm model is often given in the form of the following equation:

$$\frac{q_i}{q_{mi}} = \frac{(bP)}{(1+(bP)^n)^{1/n}} \quad (5)$$

Where q_{mi} (mol/Kg) is the maximum adsorption capacity, b (Mpa-1) and n are Toth isotherm constant. It is clear that when $n = 1$ (identical sites), this equation reduces to Langmuir isotherm equation (Tóth, 1995; Toth, 2002).

2.5.3. BET isotherm

For multilayer adsorption, BET adsorption isotherm is one of the most successful isotherm models used to express the adsorption process generated by Brunauer et al. (Brunauer et al., 1938), which assumes the interaction between the solid and the adsorbate (gas) is much larger than that between neighboring molecules. The BET equation is given by Eq.6 (Chen et al., 2017):

$$\frac{q}{q_{mi}} = \frac{bp}{(p_s-p)\left[1+(b-1)\frac{p}{p_s}\right]} \quad (6)$$

Where q_{mi}, p_s and b are the maximum loading of gas onto the surface of molecular sieves, the saturation pressure of CH_4 at experimental temperature, and the equation constant that is exponentially related to the energy of monolayer adsorption respectively.

2.5.4. Freundlich isotherm

Freundlich adsorption isotherm is an empirical equation based on the heterogeneity of the adsorbent surface. The Freundlich isotherm is represented by (Freundlich, 1906):

$$q = kp^{1/n} \quad (7)$$

Where n and k are the constants of the Freundlich equation in relationship with the heterogeneity of the adsorption surface and capacity, respectively.

2.6. Thermodynamic Studies

The determination of the adsorption mechanism is very necessary for an adsorption study. Thermodynamic parameters such as Gibbs free energy change (ΔG°), enthalpy change (ΔH°) and entropy change (ΔS°) can be explained using the adsorption mechanism. Thermodynamic parameters were estimated through the following equations (Zhou et al., 2013; Esfandian et al., 2016a):

$$\Delta G^0_{ads} = -RT\ln k \quad (9)$$

$$\ln k = \frac{\Delta S^0_{ads}}{R} - \frac{\Delta H^0_{ads}}{RT} \quad (10)$$

Where ΔG^0 (J/mol), R $(J/mol\,K)$, k (gr/mol) and T are the standard Gibbs free energy change, gas constant, the Langmuir equilibrium constant, temperature respectively; $\Delta H^0(J/mol)$ and ΔS^0 $(J/mol\,K)$ are defined asa change in standard enthalpy and entropy, respectively.

2.7. Measurement of gas Adsorption

The volumetric analysis was used to investigate the capacity of molecular sieve 13X for CH_4 sorption (Fig.1). Due to its low cost, simplicity, and easy assemblage, this quantitative analytical method is extensively adopted for the gas uptake measurements. (Colina et al., 2001; Holmes et al., 2011). The CH_4 adsorption processes were explained by details in previous work (Garshasbi et al., 2017).

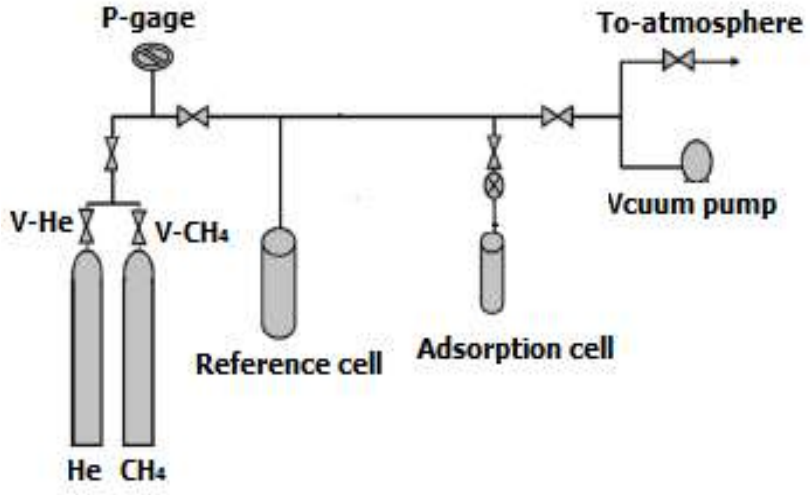

Figure 1. Volumetric set up for gas adsorption test.

3. Results and discussion

3.1. Taguchi Design of Experiment analysis

In these experiments, an L9 array design was carried out to analyze the effect of four variables of Al_2O_3/ SiO_2, Na_2O/Al_2O_3, Time (h), and Temperature (^{0}C) for the synthesis of the 13X using the Taguchi method. The relative crystallinity was selected as the test response. Fig. 2 shows the best levels for each factor obtained from each experiment (Taguchi L9 array) for the synthesis of 13X. After synthesis of the 13X zeolite powder, their properties were characterized. The synthesized powders crystallinities were considered as the desired response. Using ANOVA parameters where have significant effects on the synthesized 13X zeolite powder crystallinity can be selected. The main objective of ANOVA analysis is further investigation of the significance of the selected parameters in terms of their impact(s) on the concerned response(s), i. e. the 13X zeolite content of produced powders here. As observed from Table 3, the most affective synthesis parameter of the 13X zeolite content is the SiO_2/Al_2O_3 ratio (with minimum P-value or maximum F-value). The second and third parameters, which great impact on the 13X zeolite formation, are the Na_2O/Al_2O_3 ratio and the temperature of crystallization respectively. Finally, the duration of crystallization was found as the lowest significant effect on the synthesized zeolite crystallinity.

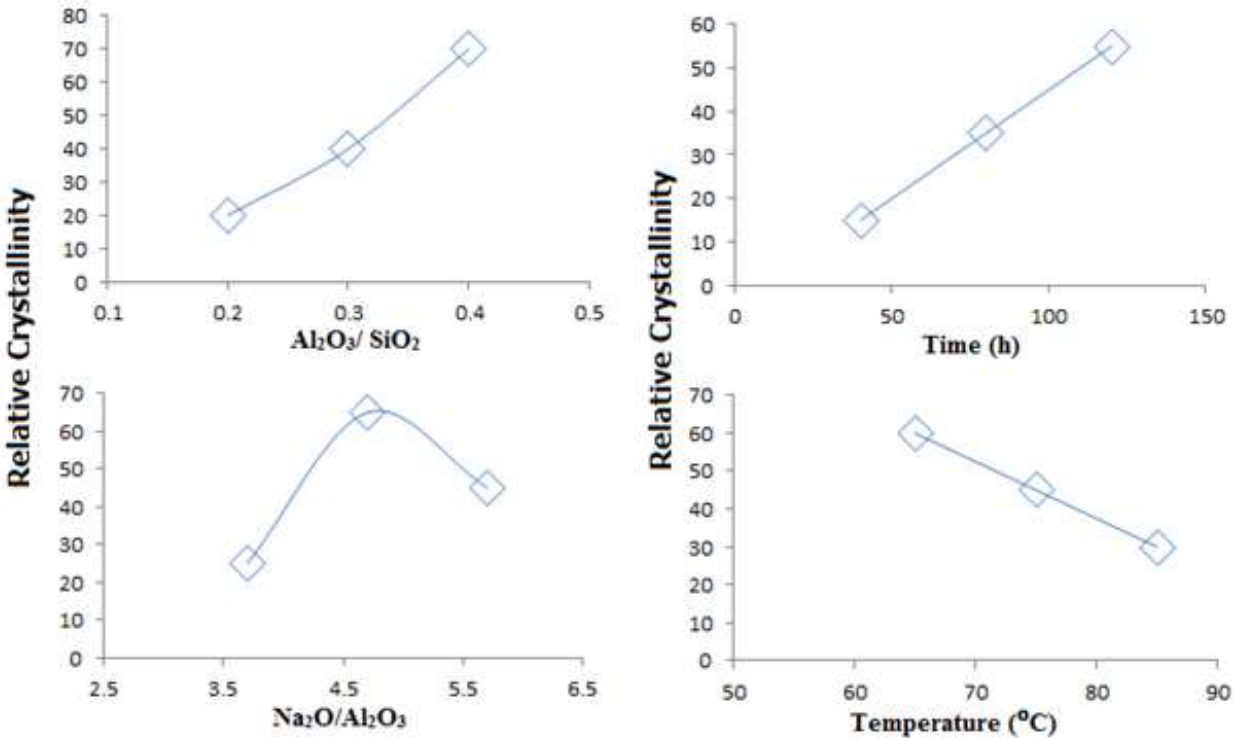

Figure 2. Best levels for selected parameters.

Table 3.Analysis of variance (ANOVA) of carried out experiments in terms of the synthesized 13X zeolite.

Kaolin				
Source	**Sum of Squares**	**Mean Square**	**F-Value**	**P-Value**
Model	3105.55	240.40	15.98	<0.0001
A - (SiO_2/Al_2O_3) ratio	770.65	770.65	58.33	<0.0001
B - (Na_2O/Al_2O_3) ratio	235.02	235.02	16.65	0.0011
C - Temperature of crystallization T(°C)	94.35	94.35	7.23	0.0242
D - Duration of crystallization T(h)	25.65	25.65	0.52	0.4735
A^2	195.89	195.89	12.47	0.0025
B^2	97.55	97.55	7.45	0.0216
C^2	350.56	350.56	23.958	0.0001
AC	180.97	180.97	11.05	0.0048
AD	350.65	350.65	25.24	0.0001
BC	128.98	128.98	8.64	0.0100
CD	86.97	86.97	4.62	0.0472
Residual	250.32	15.23		
Lack of fit	189.65	18.54	2.09	0.2231
Pure error	45.21	8.67		
Cor total	3320.20			
Bentonite				
Source	**Sum of Squares**	**Mean Square**	**F-Value**	**P-Value**
Model	3166.55	245.40	18.88	<0.0001
A - (SiO_2/Al_2O_3) ratio	780.66	780.66	59.31	<0.0001
B - (Na_2O/Al_2O_3) ratio	240.02	240.02	17.60	0.0011
C - Temperature of crystallization T(°C)	94.35	94.35	7.23	0.0232
D - Duration of crystallization T(h)	25.88	25.88	0.51	0.4695
A^2	185.80	185.80	13.57	0.0024
B^2	97.88	97.88	7.45	0.0218
C^2	360.54	360.54	23.958	0.0001
AC	190.97	190.97	11.05	0.0068
AD	347.69	347.69	25.24	0.0001
BC	133.98	133.98	8.77	0.0100
CD	77.97	77.97	4.52	0.0490
Residual	250.32	15.23		
Lack of fit	179.65	19.54	2.09	0.2231
Pure error	55.21	8.67		
Cor total	3230.20			
Feldespath				
Source	**Sum of Squares**	**Mean Square**	**F-Value**	**P-Value**
Model	3104.54	238.48	16.90	<0.0001
A - (SiO_2/Al_2O_3) ratio	670.65	670.65	59.13	<0.0001
B - (Na_2O/Al_2O_3) ratio	234.02	234.02	15.55	0.0011
C - Temperature of crystallization T(°C)	89.35	89.35	7.99	0.0292
D - Duration of crystallization T(h)	25.65	25.65	0.52	0.4835
A^2	188.89	188.89	14.87	0.0022
B^2	100.55	100.55	7.44	0.0212
C^2	354.33	354.33	22.900	0.0001
AC	181.97	181.97	12.05	0.0042
AD	370.65	370.65	29.24	0.0001
BC	133.98	133.98	9.64	0.0100
CD	86.98	86.98	8.64	0.0472
Residual	260.32	16.28		
Lack of fit	189.65	18.54	2.12	0.2288
Pure error	46.23	8.20		
Cor total	3300.20			

3.2. Characterization of Synthesis Molecular Sieve 13X

Fig.3 indicates the XRD pattern of natural kaolin, modified kaolin, bentonite, modified bentonite, feldspar, modified feldspar, and commercial molecular sieve 13X. The modification was done by giving heat to natural materials at 900 ˚C for 2 h. XRD pattern shows a significant change between modified and untreated natural materials. The characteristic peaks of synthesized products attributed to 13X are observable at 2θ values of 6.12˚, 10.00 ˚, 23.31 ˚, 26.65 ˚, 33.59 ˚, and 37.34 ˚.

The FTIR of samples is shown in Fig. 4. The results indicated that the broadband of natural materials is in the range of about 920 cm^{-1} to about 670 cm^{-1} and is related to Al-O bonds in Al_2O_3. By the reaction between NaOH and SiO_2 and Al_2O_3, aluminosilicates were

produced. The bending vibration bands in the IR spectrum were replaced by a single band around 1000 cm^{-1}, characteristic of Si–O–Al bonds (Cavenati et al., 2004).

The morphology of the natural materials and synthesized 13X are presented in Fig.5. As shown, the 13X produced from natural kaolin, bentonite, and feldspar showed that the formation of spherical micro-sized particles with an average size of 5 µm.

Figure 6 shows the TGA profile of the 13X samples. According to the results, 13X-K was more resistive to heat.

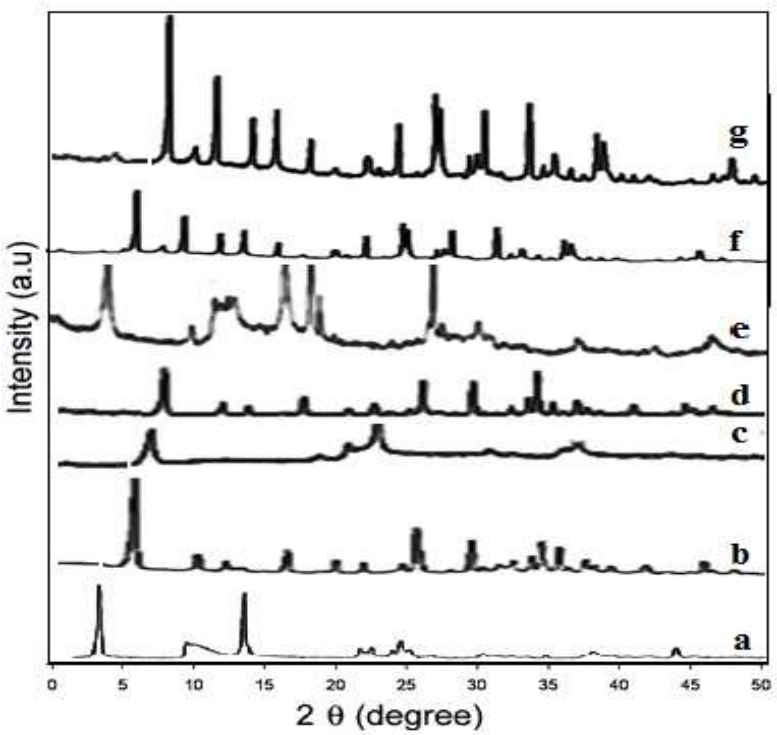

Figure 3. X-ray diffraction (XRD) pattern of the a) natural kaolin, b) modified kaolin, c) bentonite, d) modified bentonite, e) feldspar, f) modified feldspar and g) commercial molecular sieve 13X.

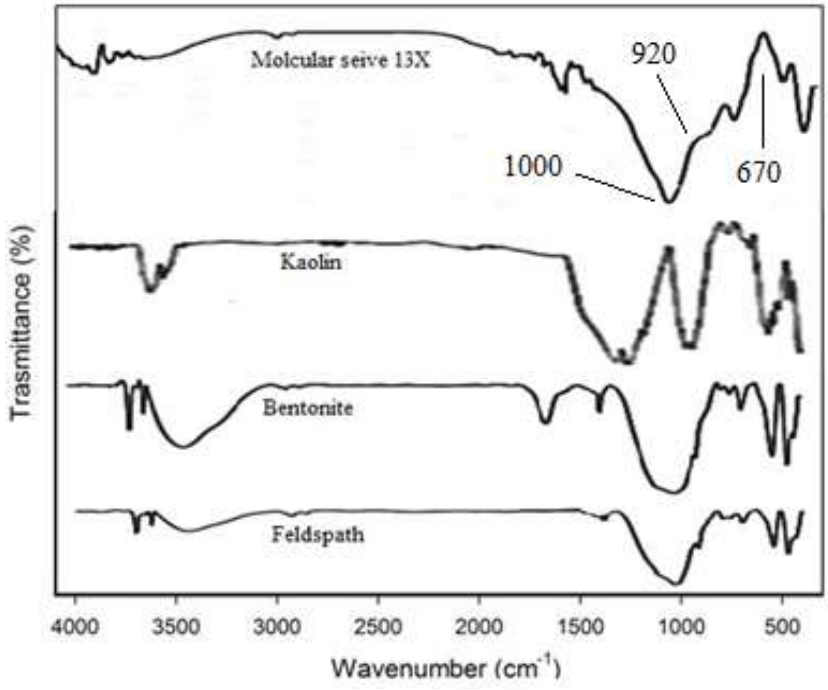

Figure 4. IR spectra of the natural kaolin, bentonite, feldspar, and molecular sieve 13X.

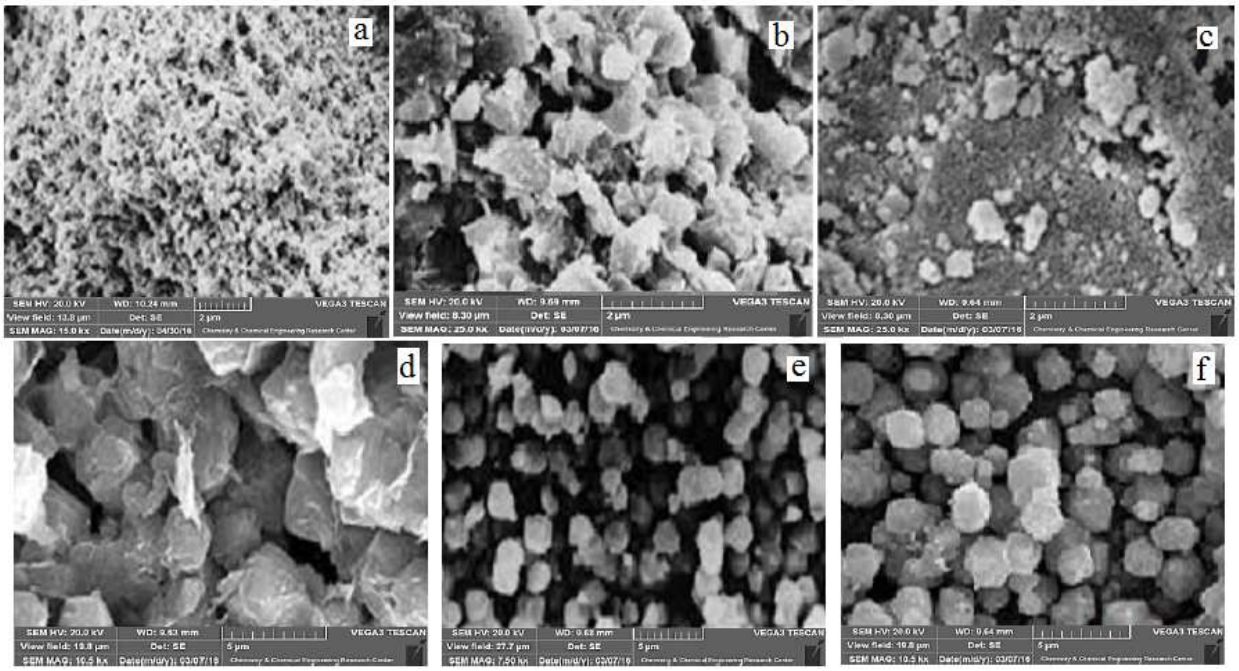

Figure5. SEM images a) natural kaolin, b) natural bentonite, c) natural feldspar, d) 13X-F,e)13X-B and f) 13X-K.

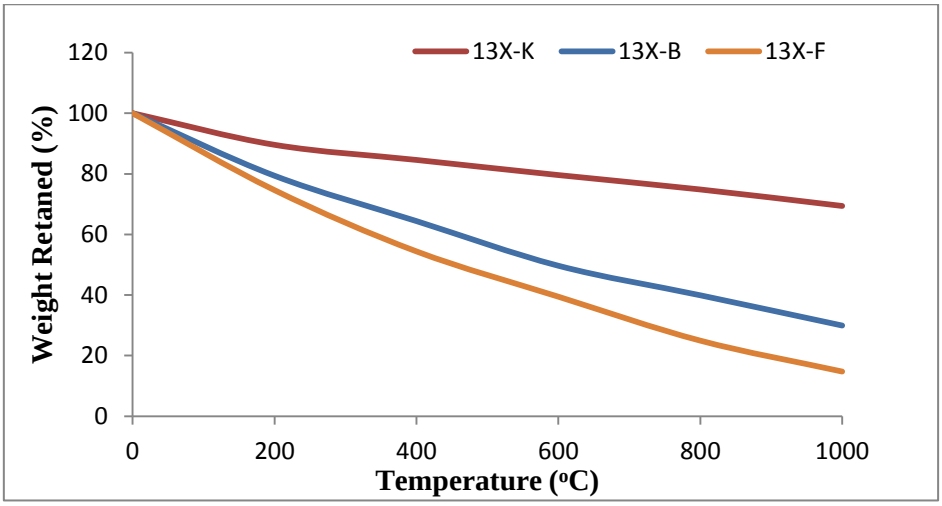

Figure 6. TGA profile of synthesized molecular sieves.

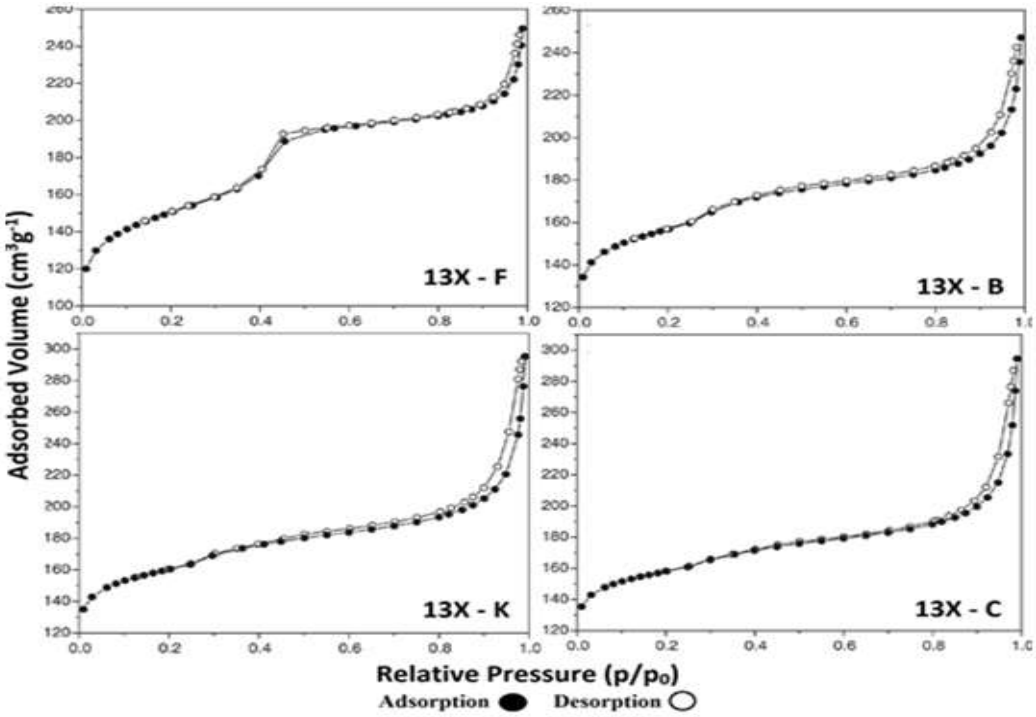

Figure 7. N2 adsorption-desorption isotherm of synthesis molecular sieves 13X prepared from kaolin (13X-K), prepared from bentonite (13X- B), prepared from feldspar (13X- F) and commercial molecular sieve 13X (13X – C).

Fig.7 shows N_2 adsorption-desorption isotherm of synthesized samples. The specific surface areas and micropore volume were determined by assuming the BET equation from the t-plot method. The BET results of synthesis molecular sieve 13X are presented in Table 4.

Table 4. Molecular sieve 13X textural properties prepared from different natural sources.

Type of molecular sieve	BET surface area (m^2/g)	Micropore surface area (m^2/g)	Micropore volume (cm^3/g)	External surface area (m^2/g)
13X-C	588	566	0.240	33
13X- K	591	576	0.250	34
13X- B	505	498	0.160	28
13X- F	472	460	0.140	26

3.3. Methane Adsorption

The synthesized 13X samples were used to adsorb the CH_4 at different temperatures (298, 308, 318, and 328 K) and pressures (Fig.8). Results show that the pore structure of molecular sieve 13X was large enough; the steric effect of the adsorbate with the adsorbent structure was ignored. As shown, there was good harmony between the experimental data of CH_4 adsorption in this study with the data found in the literature (Cavenati et al., 2004). The correlation between the CH_4 adsorption vs. pressures at different temperatures (298, 308, 318 and 328 K) for the synthesis of the molecular sieve 13X-K well fitted by following equations (Fig. 9):

$$q = -0.0142P^2 + 0.0464P \quad (11)$$
$$q = -0.012P^2 + 0.395P \quad (12)$$
$$q = -0.0085P^2 + 0.29P \quad (13)$$
$$q = -0.00675P^2 + 0.2325P \quad (14)$$

The results show that there is a fair correlation of the amount of adsorption on an adsorbent with increased adsorption for lower temperatures.

3.4. Isotherm study

The equilibrium results were modeled and evaluated through five different isotherms and error functions. Based on the maximizing the correlation factor, the comparison of the error function was made, and the best isotherm equations were found. Different isotherm parameters for different types of 13X are shown in Table 5-7. The results indicated that the Sips isotherm provided the best fit to the equilibrium data. There was a good agreement between the predicted theoretical breakthrough curves and the experimental results with Sips> Langmuir > Freundlich > Toth > BET.

Among the two-parameter isotherm models, Langmuir showed the better fitting for all

adsorbents. This clearly indicated that CH_4 adsorption took place monolayer onto the homogeneous surface of 13X, which exhibits a uniform distribution of adsorption energy. It was observed that the three-parameter isotherm models (especially Sips) fitted better with adsorption data in comparison to the two-parameter models, illustrating the complexity of the adsorption process. It can be described that Langmuir is the most reliable two-parameter isotherm model used to describe the adsorption of CH_4 on the synthesized adsorbents, while Sips fitted better based on the extra parameter that improved their flexibility and robustness. It should be mentioned that among the three-parameter isotherm models, only the q_{max} of Sips showed values close to the experimental q_e. (Fig.8). The better fitting of the Langmuir and Sips confirmed the fact that Langmuir is a special case of Sips (Adelodun et al., 2016).

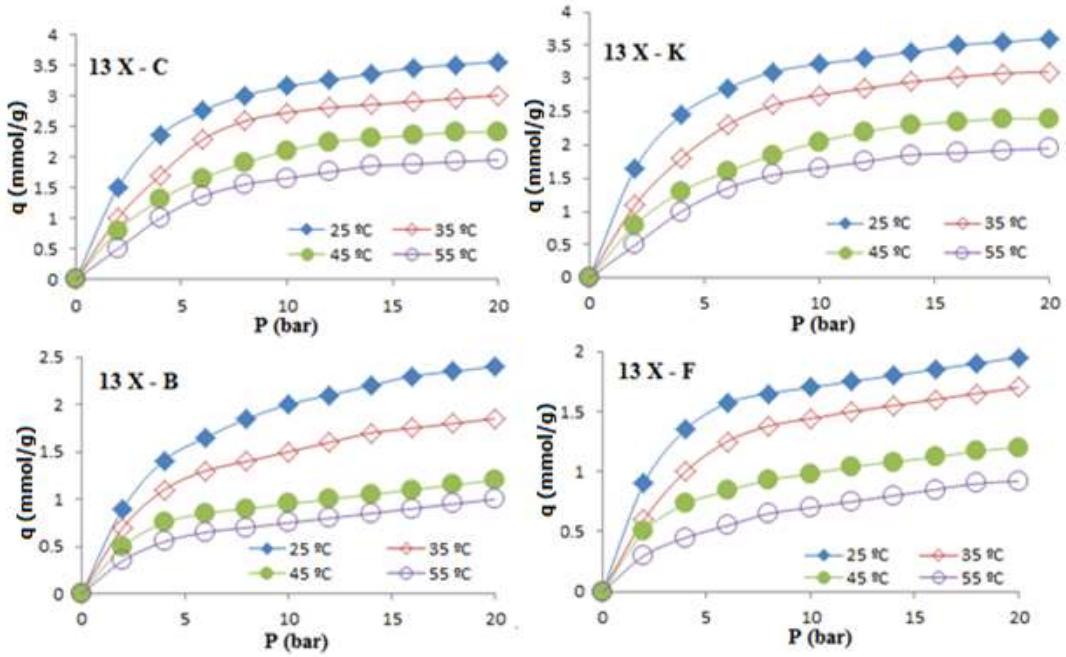

Figure 8. Experimental data of Methane adsorption on 13X synthesized molecular sieves at different temperatures.

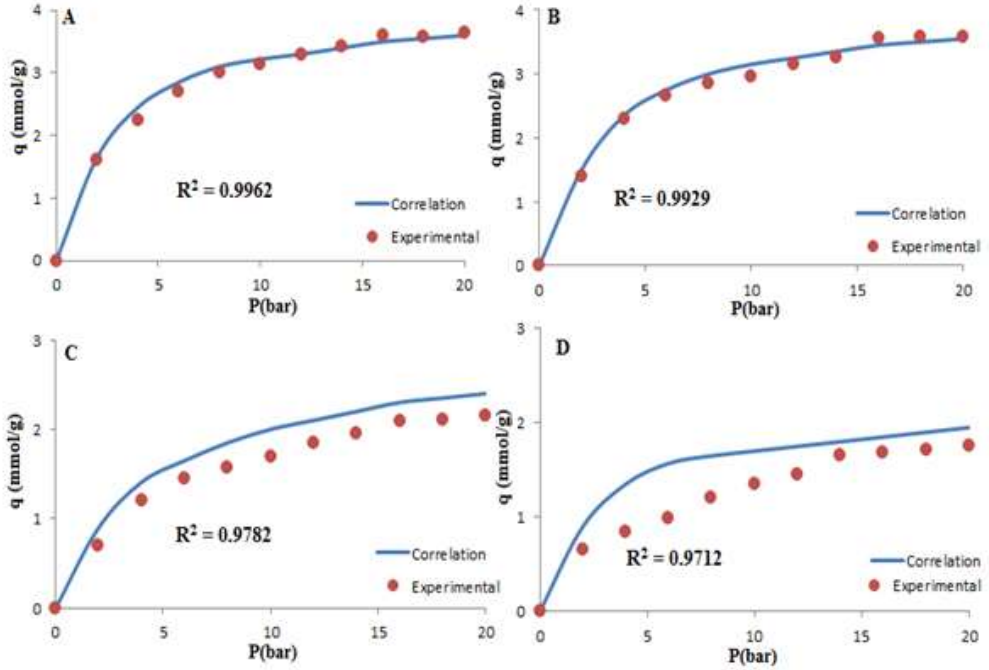

Figure 9. CH4 adsorption behavior on synthesized 13X- K at different temperatures. A) 298K (B) 308 K, (C) 318 K and (D) 328K.

Table 5. The parameters of CH4 adsorption isotherms at different temperatures on molecular sieve 13X - K

Temperature (^{0}C)	Langmuir model			
	$q_b\ (mmol/g)$	$b(\times 10^{-5})$	n	R^2
25	3.30	1.47	-	0.9820
35	3.018	1.44	-	0.9835
45	2.75	0.265	-	0.9970
55	1.65	0.201	-	0.9921
	Sips model			
25	3.62	0.85	1.23	0.9905
35	3.13	0.55	1.17	0.9914
45	2.44	0.099	1.13	0.9947
55	1.99	0.085	1.08	0.9935
	Toth model			
25	2.95	1.09	0.26	0.9798
35	2.70	0.87	0.28	0.9869
45	1.98	0.31	0.33	0.9897
55	1.85	0.21	0.39	0.9852
	BET model			
25	2.65	1.58	-	0.9692
35	2.15	1.01	-	0.9669
45	1.75	0.57	-	0.9698
55	1.35	0.35	-	0.9559
	Freundlich model			
	k	n	R^2	
25	3.07	1.64	0.9886	
35	2.82	1.20	0.9814	
45	1.50	1.12	0.9700	
55	1.45	1.01	0.9685	

Table 6. The parameters of CH4 adsorption isotherms at different temperatures on molecular sieve 13X – B

Temperature (^{0} C)	Langmuir model			
	q_b (mmol/g)	$b(\times 10^{-5})$	n	R^2
25	2.20	1.46	-	0.9833
35	1.69	1.39	-	0.9887
45	1.10	0.255	-	0.9860
55	0.98	0.211	-	0.9891
	Sips model			
25	2.47	0.79	1.43	0.9910
35	1.89	0.54	1.35	0.9917
45	1.26	0.098	1.31	0.9936
55	1.048	0.084	1.23	0.9928
	Toth model			
25	1.89	1.19	0.43	0.9789
35	1.29	0.77	0.55	0.9788
45	0.98	0.36	0.55	0.9754
55	0.81	0.29	0.6	0.9798
	BET model			
25	1.84	1.44	-	0.9622
35	1.24	1.11	-	0.9689
45	0.77	0.57	-	0.9666
55	0.40	0.50	-	0.9669
	Freundlich model			
	k	n	R^2	
25	2.33	1.59	0.9888	
35	1.58	1.22	0.9845	
45	1.01	1.17	0.9800	
55	0.93	1.09	0.9802	

Table 7. The parameters of CH4 adsorption isotherms at different temperatures on molecular sieve 13X – F

Temperature (^{0} C)	Langmuir model			
	q_b (mmol/g)	b($\times 10^{-5}$)	n	R^2
25	1.92	1.22	-	0.9908
35	1.58	1.12	-	0.9825
45	1.99	0.298	-	0.9812
55	0.88	0.211	-	0.9935
	Sips model			
25	1.96	0.89	1.67	0.9990
35	1.72	0.45	1.61	0.9955
45	1.22	0.097	1.53	0.9932
55	0.93	0.075	1.52	0.9909
	Toth model			
25	1.44	1.19	0.56	0.9791
35	1.19	0.77	0.61	0.9812
45	1.01	0.21	0.66	0.9822
55	0.75	0.19	0.87	0.9802
	BET model			
25	1.45	1.55	-	0.9729
35	1.15	1.01	-	0.9708
45	0.79	0.52	-	0.9688
55	0.69	0.33	-	0.9609
	Freundlich model			
	k	n	R^2	
25	1.78	1.71	0.9822	
35	1.66	1.35	0.9802	
45	0.94	1.21	0.9702	
55	0.56	1.08	0.9610	

3.5. Thermodynamic studies

Gibbs free energy (ΔG), the enthalpy change (ΔH), and entropy change (ΔS) for the CH_4 adsorption by 13X were calculated. So, the gas thermodynamic behavior was investigated using the change in free energy (ΔG^0), enthalpy (ΔH^0) and entropy (ΔS^0) (Eq.9-10). Table 8 presents the thermodynamic behavior of CH_4 adsorption. The positive value of ΔS^0_{ads} revealed the increased randomness at the solid-solution interface during the gas adsorption. The negative values of ΔH^0_{ads} showed the adsorption process was exothermic. Otherwise, the ΔG^0_{ads} negative values indicated the spontaneous nature of the adsorption of CH_4 on the adsorbent (Zhang et al., 2010; Chen et al., 2012a).

Table 8. Values Gibbs free energy as a function of the adsorption temperature.

Adsorbent	Temperature (°C)	ΔG^0_{ads}(kJ/mol)	ΔH^0_{ads}(J/mol),	ΔS^0_{ads}(J/mol °C)
13X- K	25	-1.59	-31.89	0.0867
	35	-1.98		
	45	-2.09		
	55	-2.27		
13X- B	25	-1.48	-28.96	0.0729
	35	-1.62		
	45	-1.89		
	55	-2.10		
13X- F	25	-1.39	-27.69	0.0702
	35	-1.79		
	45	-2.19		
	55	-2.36		

3.6. Comparison of the CH4 adsorption capacities by various sorbents

Table 9 presents the comparison of the adsorption capacity of the synthesized 13-X samples in this study to other literature. As can be seen, in this study, the adsorption capacity of 13X-K was considerably higher than 13X-B and 13X-F. In comparison to the other literature, 13X-K also indicated higher

adsorption capacity; however, its adsorption capacity was slightly lower than Acid treated carbon molecular sieve and MOF-235. This comparison and synthesis procedure (low coast (cheap chemical source of silica and alumina) and simple process for the synthesis) indicated that the 13X-K has a high potential to consider as a suitable adsorbent for CH_4 separation in the large scale.

Table 9. Comparison of the CH4 adsorption capacities by different adsorbents at 25 °C.

Adsorbent	Pressure (bar)	CH4 uptake (mmol/g)	Reference
molecular sieve 13X	1	0.38	(Bao et al., 2011b)
Zeolite 13X APG	1	0.51	(Xiao et al., 2017)
Zeolite 4A	1	0.57	(Xiao et al., 2017)
Cu-BTC110 MOF	1	> 0.5	(Knyazeva et al., 2019)
Acid treated carbon molecular sieve	1	353	(Zahedi et al., 2020)
MIL-100-Cr	5	1.56	(Lee et al., 2009)
MIL-100-Fe	5	1.1	(Lee et al., 2009)
molecular sieve HY	5	0.9	(Lee et al., 2009)
Copper MOF	1	0.3	(Bao et al., 2011a)
MIL-53 [Al]	1	0.7	(Rallapalli et al., 2011)
MOF-235	5	2.7	(Anbia et al., 2012)
molecular sieve (13X-K)	1	1.07	This work
molecular sieve (13X-B)	1	0.3	This work
molecular sieve (13X-F)	1	0.1	This work
molecular sieve (13X-K)	5	2.55	This work
molecular sieve (13X-B)	5	2.05	This work
molecular sieve (13X-F)	5	1.8	This work

4. Conclusion

Molecular sieve zeolites from modified natural Kaolin, Bentonite, and Feldespath for CH_4 adsorption in different conditions were synthesized. Synthesized zeolites were characterized by XRD, FTIR, SEM, TGA, and N_2 adsorption-desorption methods. The CH_4 removal was done by the volumetric method and the results have shown that the CH_4 sorption by synthesized molecular sieve zeolite prepared from kaoline, bentonite and feldespath were 3.6, 2.4, and 1.95 mmol/g, respectively. The data of adsorption equilibrium for CH_4 were fitted to some isotherms such as Langmuir, Freundlich, Sips, BET and Toth; it was found that the Sips model indicated the better fiting to experimental data. The synthesized samples at optimum conditions showed the higher adsorption capacity in comparison to the other literature.

Acknowledgments

The authors would like to acknowledge Amol University of Special Modern Technologies and Iran University of Science and Technology for all the support.

References

Abate, S., Barbera, K., Centi, G., Lanzafame, P., & Perathoner, S. (2016). Disruptive catalysis by zeolites. *Catalysis Science Technology*, *6*, 2485-2501.

Adelodun, A.A., Ngila, J.C., Kim, D.-G., & Jo, Y.-M. (2016). Isotherm, thermodynamic and kinetic studies of selective CO_2 adsorption on chemically modified carbon surfaces. *Aerosol Air Quality Research*, *16*, 3312-3329.

Alaie, M.M., Jahangiri, M., Rashidi, A., Asl, A.H., & Izadi, N. (2015). A novel selective H_2S sensor using dodecylamine and ethylenediamine functionalized graphene oxide. *Journal of Industrial Engineering Chemistry*, *29*, 97-103.

Alshameri, A., Yan, C., Al-Ani, Y., Dawood, A.S., Ibrahim, A., Zhou, C., & Wang, H. (2014). An investigation into the adsorption removal of ammonium by salt activated Chinese (Hulaodu) natural zeolite: kinetics, isotherms, and thermodynamics. *Journal of the Taiwan Institute of Chemical Engineers*, *45*, 554-564.

Anbia, M., Hoseini, V., & Sheykhi, S. (2012). Sorption of methane, hydrogen and carbon dioxide on metal-organic framework, iron terephthalate (MOF-235). *Journal of Industrial Engineering Chemistry*, *18*, 1149-1152.

Ansari, M., Aroujalian, A., Raisi, A., Dabir, B., & Fathizadeh, M. (2014). Preparation and characterization of nano-NaX zeolite by microwave assisted hydrothermal method. *Advanced Powder Technology*, *25*, 722-727.

Bacsik, Z., Cheung, O., Vasiliev, P., & Hedin, N. (2016). Selective separation of CO2 and CH4 for biogas upgrading on zeolite NaKA and SAPO-56. *Applied Energy*, *162*, 613-621.

Bandarchian, F., & Anbia, M. (2015). Conventional hydrothermal synthesis of nanoporous molecular sieve 13X for selective adsorption of trace amount of hydrogen sulfide from mixture with propane. *Journal of Natural Gas Science Engineering*, *26*, 1380-1387.

Bao, Z., Alnemrat, S., Yu, L., Vasiliev, I., Ren, Q., Lu, X., & Deng, S. (2011a). Kinetic separation of carbon dioxide and methane on a copper metal–organic framework. *Journal of Colloid Interface Science*, *357*, 504-509.

Bao, Z., Yu, L., Ren, Q., Lu, X., & Deng, S. (2011b). Adsorption of CO_2 and CH_4 on a magnesium-based metal organic framework. *Journal of Colloid Interface Science*, *353*, 549-556.

Blatt, H., Tracy, R., & Owens, B. (2006). Petrology: igneous, sedimentary, and metamorphic. Macmillan.

Brunauer, S., Emmett, P.H., & Teller, E. (1938). Adsorption of gases in multimolecular layers. *Journal of the American Chemical Society*, *60*, 309-319.

Cavenati, S., Grande, C.A., & Rodrigues, A.E. (2004). Adsorption equilibrium of methane, carbon dioxide, and nitrogen on zeolite 13X at high pressures. *Journal of Chemical Engineering Data*, *49*, 1095-1101.

Chen, C., Kim, J., & Ahn, W.-S. (2012a). Efficient carbon dioxide capture over a nitrogen-rich carbon having a hierarchical micro-mesopore structure. *Fuel*, *95*, 360-364.

Chen, C., Park, D.-W., & Ahn, W.-S. (2014). CO_2 capture using zeolite 13X prepared from bentonite. *Applied Surface Science*, *292*, 63-67.

Chen, D., Hu, X., Shi, L., Cui, Q., Wang, H., & Yao, H. (2012b). Synthesis and characterization of zeolite X from lithium slag. Applied Clay Science, *59*, 148-151.

Chen, Q., Tian, Y., Li, P., Yan, C., Pang, Y., Zheng, L., Deng, H., Zhou, W., & Meng, X. (2017). Study on shale adsorption equation based on monolayer adsorption, multilayer adsorption, and capillary condensation. *Journal of Chemistry*, *2017*, 1-11.

Colina, F., Esplugas, S., & Costa, J. (2001). High temperature reaction of kaolin with inorganic acids. *British Ceramic Transactions*, *100*, 203-206.

Delgado, J.A., Uguina, M.A., Gómez, J.M., & Ortega, L. (2006). Adsorption equilibrium of carbon dioxide, methane and nitrogen onto Na- and H-mordenite at high pressures. *Separation Purification Technology*, *48*, 223-228.

Esfandian, H. (2015). Removal of diazinon from aqueous solutions in batch systems using Cu-modified sodalite zeolite: an application of response surface methodology. *International Journal of Engineering*, *28*, 1552-1563.

Esfandian, H., Parvini, M., Khoshandam, B., & Samadi-Maybodi, A. (2016a). Artificial neural network (ANN) technique for modeling the mercury adsorption from aqueous solution using Sargassum Bevanom algae. *Desalination Water Treatment*, *57*, 17206-17219.

Esfandian, H., Samadi-Maybodi, A., Khoshandam, B., & Parvini, M. (2017). Experimental and CFD modeling of diazinon pesticide removal using fixed bed column with Cu-modified zeolite nanoparticle. *Journal of the Taiwan Institute of Chemical Engineers*, *75*, 164-173.

Esfandian, H., Samadi-Maybodi, A., Parvini, M., & Khoshandam, B. (2016b). Development of a novel method for the removal of diazinon pesticide from aqueous solution and modeling by artificial neural networks (ANN). Journal of Industrial Engineering Chemistry, *35*, 295-308.

Freundlich, H. (1906). Over the adsorption in solution. *The Journal of Physical Chemistry*, *57*, 1100-1107.

Garshasbi, V., Jahangiri, M., & Anbia, M. (2017). Equilibrium CO2 adsorption on zeolite 13X prepared from natural clays. *Applied Surface Science*, *393*, 225-233.

Hesas, R.H., Arami-Niya, A., Daud, W.M.A.W., & Sahu, J. (2015). Microwave-assisted production of activated carbons from oil palm shell in the presence of CO_2 or N_2 for CO_2 adsorption. *Journal of Industrial Engineering Chemistry*, *24*, 196-205.

Holmes, S.M., Khoo, S.H., & Kovo, A.S. (2011). The direct conversion of impure natural kaolin into pure zeolite catalysts. *Green Chemistry*, *13*, 1152-1154.

Kazemian, H., Naghdali, Z., Kashani, T.G., & Farhadi, F. (2010). Conversion of high silicon fly ash to Na-P1 zeolite: alkaline fusion followed by hydrothermal crystallization. *Advanced Powder Technology*, *21*, 279-283.

Knyazeva, M., Solovtsova, O., Tsivadze, A.Y., Fomkin, A., Shkolin, A., Men'shchikov, I., Pulin, A., Shiryaev, A., Vysotskii, V., &

Kiselev, M. (2019). Methane Adsorption on Cu-BTC110 Metal-Organic Framework. *Russian Journal of Inorganic Chemistry*, *64*, 1507-1512.

Ladshaw, A., Yiacoumi, S., Tsouris, C., & DePaoli, D. (2015). Generalized gas–solid adsorption modeling: Single-component equilibria. *Fluid Phase Equilibria*, *388*, 169-181.

Lee, J.-S., Kim, J.-H., Kim, J.-T., Suh, J.-K., Lee, J.-M., & Lee, C.-H. (2002). Adsorption equilibria of CO2 on zeolite 13X and zeolite X/activated carbon composite. *Journal of Chemical Engineering Data*, *47*, 1237-1242.

Lee, J.S., Jhung, S.H., Yoon, J.W., Hwang, Y.K., & Chang, J.-S. (2009). Adsorption of methane on porous metal carboxylates. Journal of Industrial Engineering Chemistry, *15*, 674-676.

Lee, S.-Y., & Park, S.-J. (2015). A review on solid adsorbents for carbon dioxide capture. *Journal of Industrial Engineering Chemistry*, *23*, 1-11.

Llano-Restrepo, M. (2010). Accurate correlation, structural interpretation, and thermochemistry of equilibrium adsorption isotherms of carbon dioxide in zeolite NaX by means of the GSTA model. *Fluid Phase Equilibria*, *293*, 225-236.

Ma, Y., Yan, C., Alshameri, A., Qiu, X., & Zhou, C. (2014a). Synthesis and characterization of 13X zeolite from low-grade natural kaolin. *Advanced Powder Technology*, *25*, 495-499.

Ma, Y., Yan, C., Alshameri, A., Qiu, X., Zhou, C., & Li, D. (2014b). Synthesis and characterization of 13X zeolite from low-grade natural kaolin. *Advanced Powder Technology*, *25*, 495-499.

Machado, N.R.C.F., & Miotto, D.M.M. (2005). Synthesis of Na–A and–X zeolites from oil shale ash. *Fuel*, *84*, 2289-2294.

Opanasenko, M.V., Roth, W.J., & Čejka, J. (2016). Two-dimensional zeolites in catalysis: current status and perspectives. *Catalysis Science Technology*, *6*, 2467-2484.

Pires, J., Saini, V.K., & Pinto, M.s.L. (2008). Studies on selective adsorption of biogas components on pillared clays: approach for biogas improvement. *Environmental Science Technology*, *42*, 8727-8732.

Purnomo, C.W., Salim, C., & Hinode, H. (2012). Synthesis of pure Na–X and Na–A zeolite from bagasse fly ash. *Microporous Mesoporous Materials*, *162*, 6-13.

Rallapalli, P., Prasanth, K., Patil, D., Somani, R.S., Jasra, R., & Bajaj, H. (2011). Sorption studies of CO_2, CH_4, N_2, CO, O_2 and Ar on nanoporous aluminum terephthalate [MIL-53 (Al)]. *Journal of Porous Materials*, *18*, 205-210.

Tanaka, H., & Fujii, A. (2009). Effect of stirring on the dissolution of coal fly ash and synthesis of pure-form Na-A and-X zeolites by two-step process. *Advanced Powder Technology*, *20*, 473-479.

Toth, J. (2002). Adsorption. CRC Press.

Tóth, J. (1995). Uniform interpretation of gas/solid adsorption. *Advances in Colloid Interface Science*, *55*, 1-239.

Tzabar, N., & ter Brake, H. (2016). Adsorption isotherms and Sips models of nitrogen, methane, ethane, and propane on commercial activated carbons and polyvinylidene chloride. *Adsorption*, *22*, 901-914.

Wajima, T., Haga, M., Kuzawa, K., Ishimoto, H., Tamada, O., Ito, K., Nishiyama, T., Downs, R.T., & Rakovan, J.F. (2006). Zeolite synthesis from paper sludge ash at low temperature (90 C) with addition of diatomite. *Journal of Hazardous Materials*, *132*, 244-252.

Wang, J.-Q., Huang, Y.-X., Pan, Y., & Mi, J.-X. (2014). Hydrothermal synthesis of high purity zeolite A from natural kaolin without calcination. *Microporous Mesoporous Materials*, *199*, 50-56.

Xiao, G., Li, Z., Saleman, T.L., & May, E.F. (2017). Adsorption equilibria and kinetics of CH 4 and N 2 on commercial zeolites and carbons. *Adsorption*, *23*, 131-147.

Zahedi, R., Ghafourian, H., Zamani, Y., Khoramnejhadian, S., & Dabbagh, R. (2020). Study of carbon dioxide and methane adsorption on carbon molecular sieves, raw and modified by waste engine oil. *Journal of the Serbian Chemical Society*, *84*, 1-11.

Zhang, Z., Zhang, W., Chen, X., Xia, Q., & Li, Z. (2010). Adsorption of CO2 on zeolite 13X and activated carbon with higher surface area. *Separation Science Technology*, *45*, 710-719.

Zhou, C., Alshameri, A., Yan, C., Qiu, X., Wang, H., & Ma, Y. (2013). Characteristics and evaluation of synthetic 13X zeolite from Yunnan's natural halloysite. *Journal of Porous Materials*, *20*, 587-594.